Original Article

MOLECULAR METABOLISM

NF-κB signaling in tanycytes mediates inflammation-induced anorexia

Mareike Böttcher [1,10], Helge Müller-Fielitz [1,9,10], Sivaraj M. Sundaram [1], Sarah Gallet [2,3], Vanessa Neve [1], Kiseko Shionoya [4], Adriano Zager [4], Ning Quan [5], Xiaoyu Liu [5], Ruth Schmidt-Ullrich [6], Ronny Haenold [7,8], Jan Wenzel [1,9], Anders Blomqvist [4], David Engblom [4], Vincent Prevot [2,3], Markus Schwaninger [1,9,*]

ABSTRACT

Objectives: Infections, cancer, and systemic inflammation elicit anorexia. Despite the medical significance of this phenomenon, the question of how peripheral inflammatory mediators affect the central regulation of food intake is incompletely understood. Therefore, we have investigated the sickness behavior induced by the prototypical inflammatory mediator IL-1β.

Methods: IL-1β was injected intravenously. To interfere with IL-1β signaling, we deleted the essential modulator of NF-κB signaling (*Nemo*) in astrocytes and tanycytes.

Results: Systemic IL-1β increased the activity of the transcription factor NF-κB in tanycytes of the mediobasal hypothalamus (MBH). By activating NF-κB signaling, IL-1β induced the expression of cyclooxygenase-2 (Cox-2) and stimulated the release of the anorexigenic prostaglandin E_2 (PGE_2) from tanycytes. When we deleted *Nemo* in astrocytes and tanycytes, the IL-1β-induced anorexia was alleviated whereas the fever response and lethargy response were unchanged. Similar results were obtained after the selective deletion of *Nemo* exclusively in tanycytes.

Conclusions: Tanycytes form the brain barrier that mediates the anorexic effect of systemic inflammation in the hypothalamus.

Keywords Tanycytes; Inflammation-induced anorexia; IL-1β; NEMO

1. INTRODUCTION

Cachexia and anorexia in chronic diseases, like HIV infection or cancer, worsen the outcome and increase mortality [1–3]. A prominent mechanism underlying cachexia is thought to be systemic inflammation [4]. Inflammation induces the so-called sickness response including fever, lethargy, and anorexia. This repertoire of physiological reactions is conserved during evolution and, in another context, seems to have a physiological benefit. Apparently, it helps mobilize the resources required to combat specific causal pathogens [5]. Infection-induced anorexia increases host tolerance to bacterial inflammation [6]. In turn, pathogens have developed the means to manipulate the host response. *Salmonella typhimurium* modulates host survival and promotes disease transmission to other subjects by interfering with the maturation of IL-1β that induces anorexia [7].

Proinflammatory cytokines such as IL-1β are essential for the host response to inflammation and infection. In accordance with this notion, IL-1β is induced by local or systemic inflammation and, when administered systemically, triggers many of the characteristic physiological changes, including anorexia, fever, and lethargy [8]. Upon binding to its membrane receptor IL-1R1 that is widely expressed in the CNS [9], IL-1β stimulates a proinflammatory signaling cascade that is mediated by the adaptor protein Myd88. In line with this, the global deletion of Myd88 prevented inflammation-induced anorexia [10,11]. Downstream of Myd88, IL-1β activates the canonical NF-κB signaling pathway that involves the protein kinase IKK complex. The latter consists of two enzymatic subunits and the essential regulatory subunit NEMO. Among the hundreds of NF-κB target genes, *Ptgs2* (*Cox-2*) stands out in the context of inflammation-induced anorexia because blocking its activity by common analgesic and antipyretic drugs, such as acetylsalicylic acid or celecoxib, reduces fever and inflammation-induced anorexia [12,13]. Thus, a precise picture of the molecular signaling pathways that mediate inflammation-induced anorexia emerges, but less is known about which cellular and anatomic routes convey the inflammatory signal to the hypothalamic centers that regulate food intake. With a molecular weight of about 17 kD, IL-1β is

[1]Institute for Experimental and Clinical Pharmacology and Toxicology, University of Lübeck, 23562, Lübeck, Germany [2]Inserm, Laboratory of Development and Plasticity of the Neuroendocrine Brain, Jean-Pierre Aubert Research Centre, U1172, Lille, France [3]University of Lille, FHU 1000 days for Health, School of Medicine, U1172, Lille, France [4]Department of Clinical and Experimental Medicine, Linköping University, S-581 85, Linköping, Sweden [5]Charles E. Schmidt College of Medicine and Brain Institute, Florida Atlantic University, Jupiter, FL, 33458, USA [6]Department of Signal Transduction in Tumor Cells, Max-Delbrück-Center (MDC) for Molecular Medicine, 13125, Berlin, Germany [7]Leibniz Institute on Aging, Fritz Lipmann Institute (FLI), 07745, Jena, Germany [8]Matthias Schleiden Institute of Genetics, Bioinformatics and Molecular Botany, Friedrich Schiller University Jena, 07743, Jena, Germany [9]DZHK (German Centre for Cardiovascular Research), partner site Hamburg/Kiel/Lübeck, Lübeck, Germany

[10] Shared first authorship.

*Corresponding author. University of Lübeck, Institute for Experimental and Clinical Pharmacology and Toxicology, Ratzeburger Allee 160, 23562, Lübeck, Germany. E-mail: markus.schwaninger@uni-luebeck.de (M. Schwaninger).

Received March 13, 2020 • Revision received May 6, 2020 • Accepted May 14, 2020 • Available online 21 May 2020

https://doi.org/10.1016/j.molmet.2020.101022

too big for unassisted diffusion through brain barriers, although there are some reports stating that small amounts of radioactively labeled IL-1β can enter the brain [14]. Endothelial cells of the blood—brain barrier are a key hub for transmitting fever inducing signals into the hypothalamus [15—18]. In marked contrast, endothelial cells do not mediate anorexia that is induced by peripheral inflammation [17,19,20].

In the MHB, tanycytes represent another barrier-forming cell type [21]. These specialized glial cells separate the vascular compartment and circumventricular organs from brain parenchyma and cerebrospinal fluid (CSF). They line the wall and floor of the 3rd ventricle in the MHB and project into the ventromedial nucleus (VMH) and arcuate nucleus (ARC), the hypothalamic centers that regulate appetite [21]. A link to metabolic regulation is further suggested by the observation that tanycytes are able to sense glucose [22] and ghrelin [23] and to transport leptin into the CNS [24]. However, their physiological function in regulating food intake still remains largely elusive.

In this study, we have investigated the cellular pathways mediating IL-1β-induced anorexia. Systemic IL-1β administration stimulated NF-κB activity in tanycytes of the MHB. To inhibit NF-κB signaling, we deleted the essential IKK subunit NEMO in glial cells and tanycytes demonstrating that IL-1β-induced anorexia at least partially depends on tanycytic NF-κB signaling. These data suggest tanycytes as an important route to transfer peripheral immune signals into the CNS and modulate the energy supply under inflammatory conditions.

2. MATERIALS AND METHODS

2.1. Animals

Animal experiments were approved by the local ethics committee (Ministerium für Energiewende, Landwirtschaft, Umwelt, Natur und Digitalisierung in Kiel, Germany; Animal Care and Use Committee at Linköping University, Sweden) and were in accordance with the EU Directive 2010/63/EU for animal experiments. For all experiments, we used male 8- to 12-week-old mice that were on a C57Bl/6 background. They were housed on a light—dark cycle of 12 h and at a temperature of 22 °C, except for body temperature measurements, which were performed under near thermoneutral conditions (29 °C). All mice had *ad libitum* access to a standard laboratory diet (2.98 kcal/g; Altromin, Hannover, Germany; 2.91 kcal/g, Lantmännen, Malmö, Sweden) and water, unless indicated otherwise. To investigate the influence of NF-κB in tanycytes under proinflammatory conditions, $Nemo^{FL}$ mice [25] were crossed with mice that express a tamoxifen-inducible Cre recombinase under the glia-specific *Glast* promoter ($GlastCreER^{T2}$) [26]. At an age of 8—10 weeks, tamoxifen was injected (1 mg, every 12 h over 5 days) to induce *Nemo* knockout in glial cells ($Nemo^{gliaKO}$). Tamoxifen-treated Cre-negative littermates were used as controls ($Nemo^{FL}$). NF-κB reporter mice (κ-EGFP) [27] and $Il1r1^{GR/GR}$ reporter mice [28] have been described previously. To specifically delete *Nemo* in tanycytes, a rAAV approach was used that we have recently developed [29]. We tested the cell specificity of AAV-Dio2-iCre-2A-EGFP and $GlastCreER^{T2}$ with the Cre reporter mouse line Ai14 [30]. All mice were randomly allocated to treatment groups. Investigators were blinded for treatment or genotype of mice or both whenever possible. Mice were only excluded from analysis if they did not survive during surgical procedures or if samples could not be obtained.

2.2. Primary tanycyte cell culture

Tanycytes were isolated from P10 Sprague Dawley rats (Janvier) by dissecting the wall of the 3rd ventricle of the MBH as described previously [31]. A tanycyte cell culture contained tissue from 20 pups, which had been collected in culture medium (DMEM high-glucose medium containing 10% fetal calf serum, 1% penicillin/streptomycin, and 2 mM L-glutamine, Thermo Fisher) on ice. To separate tanycytes, samples were scraped through a nylon mesh (20 μm, Merck Millipore) and centrifuged, and cells were resuspended in a fresh culture medium. No medium change was done within the first 10 days; afterward, the medium was changed twice a week. Cultures that reached confluency were split by trypsin/ETDA digestion and plated in 6-well plates for further experiments. After 3 weeks, the medium of the cultures was changed to starvation medium (DMEM/F12 without phenol red, 1% penicillin/streptomycin, and 2 mM L-glutamine, all from Thermo Fisher). One hour before the experiment started, cells were changed to experimental medium (DMEM/F12 without phenol red, 1% penicillin/streptomycin, 2 mM L-glutamine (all from Thermo Fisher), and 0.15% insulin and 0.3% putrescine (last two from Sigma—Aldrich, USA)) and treated with rat recombinant IL-1β (0.25 μg/mL, Peprotech) or PBS. Cells were harvested after 0, 2, 4, 8, and 24 h by washing them 3 times with ice-cold PBS and shock freezing on dry ice. The purity of the primary cell culture was confirmed by immunostaining of vimentin, GFAP, and CD11b as well as by qRT-PCR.

To inhibit NF-κB, tanycytes were treated prior to the experiment with 25 μM BMS-345541 (dissolved in DMSO, Axon Medchem BV) or 0.25% DMSO. After 30 min, cells were treated with rat recombinant IL-1β (0.25 μg/mL, Peprotech). The supernatant was collected after 2 and 8 h of treatment, and the cells were harvested. Secreted prostaglandin E2 was measured by using the Prostaglandin E2 Elisa Kit (Cayman) according to the manufacturer's instructions.

2.3. AAV production and stereotaxic vector injections

AAV with a mosaic capsid of serotypes 1 and 2 (1:1) was generated as described and purified by AVB Sepharose affinity chromatography [29]. For each vector, the genomic titer was determined by quantitative PCR (qPCR) using primers against WPRE (WPRE forward primer: 5′-TGC CCG CTG CTG GAC-3'; WPRE reverse primer: 5′-CCG ACA ACA CCA CGG AAT TG-3′) as described previously [29]. For stereotaxic injections, $Nemo^{FL}$ mice were anesthetized with ketamine (65 μg/g, Ketavet™, Pfizer) and xylazine (14 μg/g, Rompun™, Bayer) before they were fixed in the stereotaxic frame (David Kopf Instruments). During the procedure, the body temperature was maintained at 37 °C by a heating plate. After drilling a small borehole between bregma and lambda, AAV vectors (10^{11} genomic particles in 2 μL) were injected into the lateral ventricle (anteroposterior −0.1 mm, mediolateral −0.7 mm, and dorsoventral from the skull surface −2.3 mm relative to bregma) as described previously [29]. Injections were performed over 5 min and the cannula stayed in place for another 10 min to avoid backflow of the vectors. The scalp was sutured and the animals were treated with carprofen (5 mg/kg; s.c.) for 2 days. $Nemo^{FL}$ mice received either AAV-Dio2-Cre-2A-EGFP to express the Cre recombinase under the tanycytic specific *Dio2* promoter ($Nemo^{tanKO}$) or the control vector AAV-Dio2-EGFP without Cre activity ($Nemo^{Con}$).

2.4. IL-1β effects on feeding and related parameters

Mice received PBS and, after a lag time of 2 days, recombinant mouse IL-1β (20 μg/kg, i.v., Peprotech). Both treatments were administered by injection into the tail vein under anesthesia (4% isoflurane) 1 h before the lights were turned off. At the same time, the food was removed and returned at the beginning of the dark phase. Food and water intake as well as body weight, respiratory exchange ratio (RER), and energy expenditure (EE) were monitored over 24 h by indirect calorimetry.

2.5. Measurement of cytokine concentrations in plasma

For measuring cytokine concentrations in plasma, *Nemo*^{FL} and *Nemo*^{gliaKO} mice were treated with IL-1β (20 μg/kg, i.v., Peprotech) and were sacrificed after 4, 8, and 24 h by a lethal dose of pentobarbital (150 μg/g, i.p.). Blood samples were obtained by heart puncture in EDTA vials (Sarstedt). IL-1β, IL-6, and TNF were measured in plasma by MILLIPLEX mouse kit (Merck Millipore) according to the manufacturer's instructions.

2.6. Reporter mice for monitoring NF-κB activation and *Il1r1* expression

κ-EGFP mice were used to identify cells with NF-κB activity in the MBH after IL-1β treatment. Therefore, κ-EGFP mice were treated either with mouse recombinant IL-1β (20 μg/kg, i.v.) or with PBS under 4% isoflurane anesthesia. Eight hours later, mice were sacrificed by a lethal dose of pentobarbital (150 μg/g, i.p.). Brains were postfixed in paraformaldehyde (PFA, 4%), cryoprotected by incubation in sucrose (30% in PBS) for 24 h, and stored at −80 °C. We counted EGFP-positive cell bodies.

To localize *Il1r1* expression, we used *Il1r1*$^{GR/GR}$ mice [28]. To enhance IL-1R1 expression, the animals were treated with LPS (120 μg/kg, *E. coli* serotype 0111:B4, i.p.) and perfused after 6 h with 0.9% saline at room temperature, followed by ice-cold PFA (4%, pH 9.5). Brains were postfixed for 2 h and cryoprotected for 48 h.

2.7. Telemetric monitoring of mice

Two weeks after inducing recombination with tamoxifen, mice were anesthetized with isoflurane, and transmitters (TA-F10, Data Science International) were intraperitoneally implanted. For postoperative pain management, we administered carprofen (5 mg/kg, s.c.) every 12 h for 2 days. Seven days after implanting transmitters, mice were treated with IL-1β (20 μg/kg, i.v.) 3 h after the lights were turned on and the body temperature and activity were monitored.

Novelty stress was evaluated during animal care. After *Nemo*^{FL} and *Nemo*^{gliaKO} mice carrying telemetric transmitters were transferred to new cages during the inactive light phase, body temperature and activity were recorded.

2.8. Indirect calorimetry

For indirect calorimetry 3 weeks after tamoxifen (*Nemo*^{FL} and *Nemo*^{gliaKO}) or virus injection (*Nemo*^{Con} and *Nemo*^{tanKO}), mice were kept in ventilated cages of the PhenoMaster System (TSE, Germany) for 7 days on a 12 h light/dark cycle at 23 °C. After 3 days of adaption, PBS and two days later IL-1β (20 μg/kg, i.v.) were intravenously injected 1 h before lights were turned off according to the same protocol as described above. Food and water intake were automatically monitored every 30 min. O_2 and CO_2 concentrations in the cages were measured every 30 min to determine EE and RER. All measurements ran simultaneously. EE was calculated as $3.941 \times O_{2\ \text{consumed}}$ [l] $+ 1.106 \times CO_{2\ \text{produced}}$ [l]. The measurements after PBS treatment served as intraindividual controls for the IL-1β treatment.

2.9. Isolation of tanycytes and RT-PCR

For laser microdissection, native coronal cryosections (25 μm thick) of the MBH were mounted on membrane slides 1.0 PEN (Zeiss, Germany). Tanycytes were microdissected using the Axiovert 200 M microscope (Zeiss, Germany) and a system with a pulsed 337 nm UV laser (PALM MicroBeam, PALM Microlaser Technologies) and the laser-pressure catapulting mode. Areas corresponding to α-tanycytes (about 10,000 μm^2) and to the ARC (about 60,000 μm^2) were dissected on 8 sections of the MBH (bregma −1.58 mm to −1.7 mm) and pooled. RNA was isolated using the Absolutely RNA Nanoprep Kit (Agilent Technologies) according to the manufacturer's instructions. RNA was transcribed into cDNA by the reverse transcriptase AMV (Avian Myeloblastosis Virus; Cloned AMV First-Strand cDNA Synthesis Kit, Invitrogen) with oligo(dT) primers and diluted 1:1 in diethyl pyrocarbonate (DEPC) water (Sigma—Aldrich). For real-time PCR, the following primers were used: *Ptgs2* forward primer 5′-CTG ACC CCC AAG GCT CAA AT-3′, *Ptgs2* reverse primer 5′-AAG TCC ACT CCA TGG CCC AG-3′, PCR product 124 bp; *Agrp* forward primer 5′-CGC TTC TTC AAT GCC TTT TGC-3′, *Agrp* reverse primer 5′-ATT CTC ATC CCC TGC CTT TGC-3′, PCR product 108 bp; *Npy* forward primer 5′-TCG CTC TAT CTC TGC TCG TGT G-3′, *Npy* reverse primer 5′-AGT ATC TGG CCA TGT CCT CTG C-3′, PCR product 105 bp; *Pomc* forward primer 5′-AGC GTT ACG GTG GCT TCA TGA-3'; *Pomc* reverse primer 5′-TGG AAT GAG AAG ACC CCT GCA-3′, PCR product 125 bp; and *Gapdh* forward primer 5′-CCT ACC CCC AAT GTA TCC GTT-3′, *Gapdh* reverse primer 5′-TAG CCC AGG ATG CCC TTT AGT-3′, PCR product 122 bp. Real-time PCR was performed with the Platinium SYBR Green qPCR SuperMix (Invitrogen) according to the following protocol: 2 min at 50 °C, 2 min at 95 °C, 15 s at 95 °C, and 1 min at 60 °C (40 cycles). Quantified results were normalized to *Gapdh* using the ΔΔCt method.

From primary rat tanycytes, RNA was extracted with the help of NucleoSpin columns (Macherey—Nagel). For quantification of gene expression, the following primers were used: *Ptgs2* forward primer 5′-CTC AGC CAT GCA GCA AAT CC-3′, *Ptgs2* reverse primer 5′-GGG TGG GCT TCA GCA GTA AT-3′, PCR product 172 bp; *Il1b* forward primer 5′-GGC TTC CTT GTG CAA GTG TC-3′, *Il1b* reverse primer 5′-CCC AAG TCA AGG GCT TGG AA-3′, PCR product 152 bp; *Il1r1* forward primer 5′-TGT GGC TGA AGA GCA CAG AG-3′, *Il1r1* reverse primer 5′-TGG ATC CTG GGT CAG CTT C-3′, PCR product 172 bp; *Vcam1* forward primer 5′-GGA AAT GCC ACC CTC ACC TT-3′, *Vcam1* reverse primer 5′-AAC AGT AAA TGG TTT CTC TTG AAC A-3′, PCR product 132 bp; and *Gapdh* forward primer 5′-CCT ACC CCC AAT GTA TCC GTT-3′, *Gapdh* reverse primer 5′-TAG CCC AGG ATG CCC TTT AGT-3′, PCR product 122 bp.

For the FACS of tanycytes, we used a protocol reported previously [32]. Briefly, tanycytes were labeled by injecting the Tat-Cre fusion protein in the third ventricle of Ai14 reporter mice. Then, Tomato-positive tanycytes and Tomato-negative other cells were sorted. RNA obtained from FACS-sorted cells was reverse transcribed using the High-Capacity cDNA Reverse Transcription Kit (4374966, Life Technologies), and a linear preamplification step was performed using TaqMan PreAmp Master Mix (4488593, Life Technologies). Real-time PCR was carried out on Applied Biosystems 7900 HT Fast Real-Time PCR System using the following exon-boundary-specific TaqMan Gene Expression Assays (Applied Biosystems): *Il1r1*, Mm00434237_m1; *Il1b*, Mm00434228_m1; *Ikbkg*, Mm00494927_m1; *Nfkb1*, Mm00476361_m1; *Ptgs2*, Mm00478374_m1; *Vcam1*, Mm01320970_m1; *Vimentin*, Mm01333430_m1; *Darpp32* (*Ppp1r1b*), Mm00454892_m1; *Gpr50*, Mm00439147_m1; *Gfap*, Mm01253033_m1; *Npy*, Mm03048253_m1; *Pomc*, Mm00435874_m1; *r18S*, Mm03928990_g1; *Actb*, Mm00607939. Gene expression data were analyzed using SDS 2.4.1 and DataAssist 3.0.1 software (Applied Biosystem).

2.10. Western blotting

Primary tanycytes were lysed with 1% cell lysis buffer (Cell Signaling) supplemented with phenylmethylsulfonyl fluoride (PMSF, 0.5 M Sigma—Aldrich). Protein concentrations in the lysates were measured with the Lowry assay. After SDS-PAGE, proteins were transferred to nitrocellulose membranes that were incubated with primary antibodies against COX-2 (1:250, sc-1747, Santa Cruz) and GAPDH (1:2,500, ab9485, Abcam) at 4 °C overnight followed by incubation with

secondary antibodies (1:2,500 HRP-labeled anti-goat IgG, DakoCytomation, Denmark; 1:5,000 HRP-labeled anti-rabbit IgG, Santa Cruz) at room temperature for 1 h. Detection was achieved by chemiluminescence (SuperSignal West Femto Substrate, Thermo Scientific) and a digital detection system (Fusion Solo S, VWR International).

2.11. Immunohistochemistry

To visualize NF-κB activation, serial coronal cryosections (25 μm thick) of NF-κB reporter mice (κ-EGFP) in the area of the ME (bregma −1.35 to −2.46 mm) were processed for immunohistochemistry. First, PFA-fixed sections were washed twice with Tris-buffered saline (TBS; Tris 50 mM; NaCl, 150 mM; pH 7.6) for 5 min at room temperature and incubated in TBS containing 0.3% Triton-X100 (TBST, Promega) for 15 min for permeabilization and then in TBST containing 5% BSA (Sigma—Aldrich) for 30 min at room temperature. Subsequently, samples were incubated overnight at 4 °C with primary antibodies: anti-GFP, 1:500 (ab13970, Abcam); anti-vimentin, 1:500 (5741, New England Biolabs); anti-GFAP, 1:500 (Z033429-2, Dako); anti-Iba1, 1:500 (019-19741, Wako); and anti-collagen-IV 1:1,000, (Abcam #ab6586). Finally, sections were incubated with secondary antibodies: Alexa 488-labeled goat anti-chicken, 1:5,000 (Abcam); CyTM3-conjugated donkey anti-rabbit, 1:1,000 (Jackson/Dianova); and Dapi (1 μg/mL, Sigma—Aldrich) for 1 h at room temperature.

Frozen cryosections of $Nemo^{FL}$ and $Nemo^{glialKO}$ mice were fixed in methanol for 10 min at −20 °C, washed three times with PBS, and incubated in PBS containing 1% BSA for 45 min at room temperature. Subsequently, primary antibodies were added: anti-VCAM1 at 1:1,000 (550547, BD Pharmingen) overnight at 4 °C. Then, sections were washed with PBS three times before incubation with secondary antibodies: Alexa 488-labeled anti-rat IgG at 1:1,000 (A-21208, Invitrogen) for 45 min at room temperature. Finally, sections were covered using Mowiol and a coverslip. Pictures were taken with the confocal microscope SP5 (Leica) and 10× or 20× objectives. For the quantification of VCAM1, the mean gray value of an area of 458 mm^2 was determined using ImageJ software (National Institutes of Health). All sections were stained in parallel and measured with the same settings. For detecting the reporter tdTomato in $Il1r1^{GR/GR}$ mice, 30 μm free-floating sections were incubated overnight in rabbit anti-RFP at 1:1,000 (Abcam) in PBS containing 2% normal donkey serum and 0.3% Triton X-100. Then, sections were incubated for 2 h at room temperature in secondary antibodies: Alexa 555-labeled donkey anti-rabbit IgG, 1:1,000 (Life Technologies).

To analyze the specificity of the AAV-based targeting of tanycytes, Ai14 mice were perfused with 4% PFA two weeks after injecting AAV-Dio2-Cre-2A-EGFP (5×10^{10} genomic particles) into the lateral ventricle. To investigate recombination specificity in $GlastCreER^{T2}$ mice, we treated $GlastCreER^{T2}$::Ai14 mice with tamoxifen. Brains were postfixed in 4% PFA at 4 °C overnight. For staining, free-floating sections (50 μm) were washed twice in TBS, permeabilized in TBST for 30 min, and incubated in TBST containing 5% BSA for 2 h. Then, sections were incubated in primary antibodies: anti-GFAP, 1:500, (Z033429-2, Dako); anti-CD11b, 1:500 (557397, BD Pharmingen); anti-ppTRH, 1:2,000 (a gift of Martin Wessendorf); and NeuN, 1:500, (MAB377, Millipore) overnight and in Alexa 488-labeled anti-rabbit IgG (1:500, Invitrogen #A-21206) or anti-mouse IgG (1:400, A-31619, Invitrogen) for 2 h. They were mounted as described above.

For COX-2 staining, mice were perfused with a solution containing 2% PFA and 0.2% glutaraldehyde. For antigen retrieval, vibratome sections (50 μm thick) of the MBH were incubated in sodium citrate buffer (10 mM, pH 6, 85 °C) for 30 min followed by H_2O_2 treatment (1%, 30 min). After blocking with BSA (5% in PBS + 0.3% Triton-X100) for 2 h, samples were incubated overnight at 4 °C with anti-COX-2 (M17-R, Santa Cruz, 1:1,000). Then, biotinylated secondary antibodies against rabbit IgG (1:250, Vector, BR1000) were added for 2 h. For detection, we used DAB amplification (A/B Kit, Vector; DAB-Kit, Vector). All sections were stained in parallel and incubated for 1.5 min in the DAB + nickel solution.

2.12. *In situ* hybridization for *Nemo* mRNA

The *in situ* hybridization for *Nemo* mRNA was performed with the RNAscope® Multiplex Fluorescent Reagent Kit v2 (Advanced Cell Diagnostics, ACD, Hayward, CA, USA). We used a set of 20 double Z probes targeting the first 6 exons of *Nemo* (nucleotides 246-1135 in NM_001136067) which include exon 2 that is floxed in $Nemo^{FL}$ animals [25]. Briefly, 20 μm mouse brain cryosections were postfixed at room temperature in freshly prepared 4% PFA for 15 min, dehydrated with ethanol, backed for 30 min at 37 °C, and treated with hydrogen peroxide and protease IV. Then, the sections were incubated with double Z probes for 2 h at 40 °C and hybridized sequentially by preamplifiers, amplifiers, and HRP-labeled oligonucleotides, followed by TSA® Plus Cyanine 3 probe. Nuclei were counterstained with Dapi. We mounted sections with Fluoromount (ACD). After *in situ* hybridization, the sections were imaged with the confocal microscope Leica TCS SP5. Scoring of the *Nemo* mRNA signal in the tanycyte layer of the 3rd ventricle was performed according to the manufacturer's scoring guideline (ACD). The *Nemo* mRNA signal scoring was done as follows: score 1 if 1—3 dots/cell and score 2 if 4—9 dots/cell [33]. In at least 4 sections per animal, the $Nemo^{+}$ cells were counted in the tanycytic layer. A blinding strategy was followed while scoring the RNAscope images.

2.13. Statistical analysis

All data are presented as means ± standard error of the mean (SEM). For statistical comparison of two groups, we used the Mann—Whitney test, unless the sample size per group was bigger than 9 and values were normally distributed. In this case, a *t*-test was applied. For more than two groups, the analysis was performed by one-way ANOVA with subsequent Bonferroni post hoc test or Friedman test. Time-dependent data were analyzed with two-way repeated-measures ANOVA followed by Bonferroni post hoc test. A P value < 0.05 was considered statistically significant. G-Power (Version 3.1.8) was used to analyze power and group size for the experiments.

3. RESULTS

3.1. IL-1β directly stimulates NF-κB activity in tanycytes *in vivo*

To determine in which cells of the MBH systemic IL-1β induces NF-κB activity, we injected IL-1β (20 μg/kg, i.v.) into NF-κB-EGFP reporter (κ-EGFP) mice, expressing the enhanced green fluorescent protein (EGFP) under the control of an artificial NF-κB promoter [27]. After IL-1β administration, EGFP expression was pronounced in vimentin-positive tanycytes projecting mainly in the VMH (α1-tanycytes) and few tanycytes projecting into the ventromedial ARC (vmARC) (dorsal β1-tanycytes, Figure 1A,B) but not in tanycytes projecting to the capillary bed of the median eminence (ME) (ventral β1-and β2-tanycytes, Figure 1A,C) or the dorsomedial ARC (α2-tanycytes). Counting of $EGFP^{+}$ tanycytes revealed a significant increase after IL-1β injection in comparison to the PBS-treated control group (Figure 1D). Additional EGFP expression was detectable in Iba1-positive microglia and blood vessels. Only a few GFAP-positive astrocytes in the ME were positive for EGFP (Supplementary Figure 1).

Since we had observed that systemic IL-1β stimulates NF-κB activity in tanycytes, we wondered whether IL-1β is able to directly act on

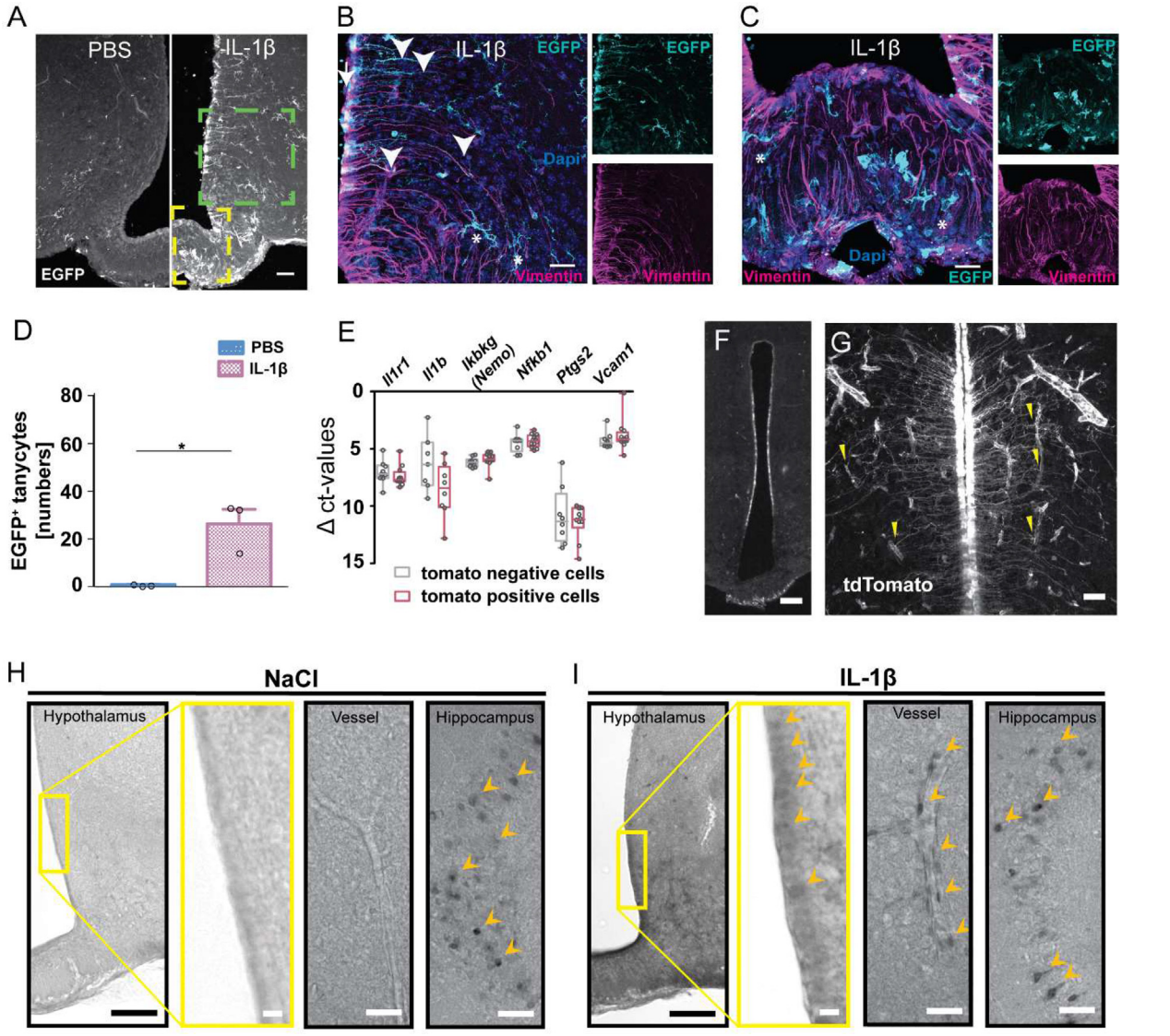

Figure 1: Systemic IL-1β activates NF-κB in tanycytes. (A) Representative immunostainings of the mediobasal hypothalamus (MBH) of κ-EGFP reporter mice 8 h after IL-1β (20 μg/kg, i.v.) or PBS injection. EGFP (A, white; B and C, cyan) reflecting NF-κB activity (cell bodies, arrow; projections, arrowheads) of tanycytes (vimentin, magenta). Asterisks indicate $EGFP^+$ microglia. Scale bar, 100 μm. (B, C) Higher magnification of the boxed area in A (green box, B; yellow box, C). Scale bar, 20 μm. (D) The number of $EGFP^+$ tanycytes in the MBH per section. Means ± SEM $^*P < 0.01$ (Mann–Whitney test, n = 3 sections/mouse of 3 mice/group). (E) mRNA expression of various genes of the IL-1β signaling pathway in FACS-sorted tanycytes (red, tdTomato-positive) and non-tanycytic cells (gray, tdTomato-negative). Medians ± quartiles. (F, G) tdTomato immunostainings (white) in tanycytes of *Il1r1*$^{GR/GR}$ mice indicating *Il1r1* transcription. Staining was performed 6 h after LPS treatment (120 μg/kg, i.p.). Yellow arrowheads indicate contact points of tanycytic endings and blood vessels. Scale bar, 150 μm (F) and 20 μm (G). (H, I) Representative COX-2 immunostainings 8 h after i.v. injection of NaCl (H) or IL-1β (20 μg/kg, I). In the hippocampus, positive cells could be identified after NaCl injection. After IL-1β treatment, COX-2-positive cells were detectable in the tanycytic layer and bigger blood vessels (I). Arrowheads, COX-2-positive cell bodies; yellow box, magnified field; scale bar, 100 μm (hypothalamic overview), 50 μm (vessels, hippocampus), and 10 μm (magnified field).

tanycytes. Using *in situ* hybridization, a previous study reported a low mRNA signal for *Il1r1*, the essential IL-1 receptor, in the tanycytic layer [34]. However, *in situ* hybridization may not be sensitive enough for the detection of all functionally relevant *Il1r1* expression, as less than 10 IL-1R1 molecules per cell are sufficient to mediate an effect of IL-1β [35]. In tanycytes that were sorted from the MBH of mice, we detected mRNA of various components of the IL-1 signaling pathway, including *Il1r1*, at similar levels as in non-tanycytic cells (Figure 1E and Supplementary Figure 2). Using *Il1r1* reporter mice (*Il1r1*$^{GR/GR}$) [28], in which the *Il1r1* locus drives expression of the reporter tdTomato, we confirmed *Il1r1* expression by detecting tdTomato-positive cells in the wall of the 3rd ventricle that projected into VMH and DMH, corresponding to the main localization of NF-κB activity in α1-tanycytes after IL-1β stimulation (Figure 1F). These cells had a typical tanycytic cell shape (Figure 1G).

IL-1β is known to upregulate COX-2 in endothelial cells of the BBB [36]. To test whether IL-1β also induces COX-2 in tanycytes, we stained sections 8 h after the vehicle and IL-1β injection. As reported previously, COX-2 was found in cells of the hippocampus and in endothelial cells of IL-1β-treated animals with a perinuclear

distribution [36,37] corroborating the specificity of the staining. Interestingly, IL-1β treatment led to weak but distinct staining of cells in the tanycytic layer (Figure 1H,I).

3.2. Tanycytes express proinflammatory genes after IL-1β stimulation

In line with the notion that tanycytes are sensitive to IL-1β, we also detected *Il1r1* mRNA in cultured primary tanycytes by RT-PCR (Figure 2A). Interestingly, IL-1β (0.25 μg/mL) enhanced its own expression, which is controlled by NF-κB (Figure 2B), as well as the NF-κB target gene vascular cell adhesion molecule 1 (*Vcam1*) (Figure 2C). In accordance with the *in vivo* findings (Figure 1H,I), IL-1β treatment induced the mRNA levels of the immediate-early gene *Ptgs2* encoding COX-2 already after 2 h (Figure 2D). At the protein level, COX-2 was significantly upregulated with a more prolonged time course (Figure 2E,F).

To test whether IL-1β enhances COX-2 levels through NF-κB-dependent signaling, primary tanycytes were treated with the IKK specific inhibitor BMS-345541 (25 μM) [38] 30 min before adding IL-1β (0.25 μg/mL). BMS-345541 almost completely suppressed COX-2 induction by IL-1β in primary tanycytes (Figure 2G,H) confirming that NF-κB signaling mediates the effect of IL-1β. Tanycytes are able to release prostaglandins, such as PGE_2 [31,39–41]. To address the functional relevance of COX-2 in tanycytes, we measured PGE_2 in the

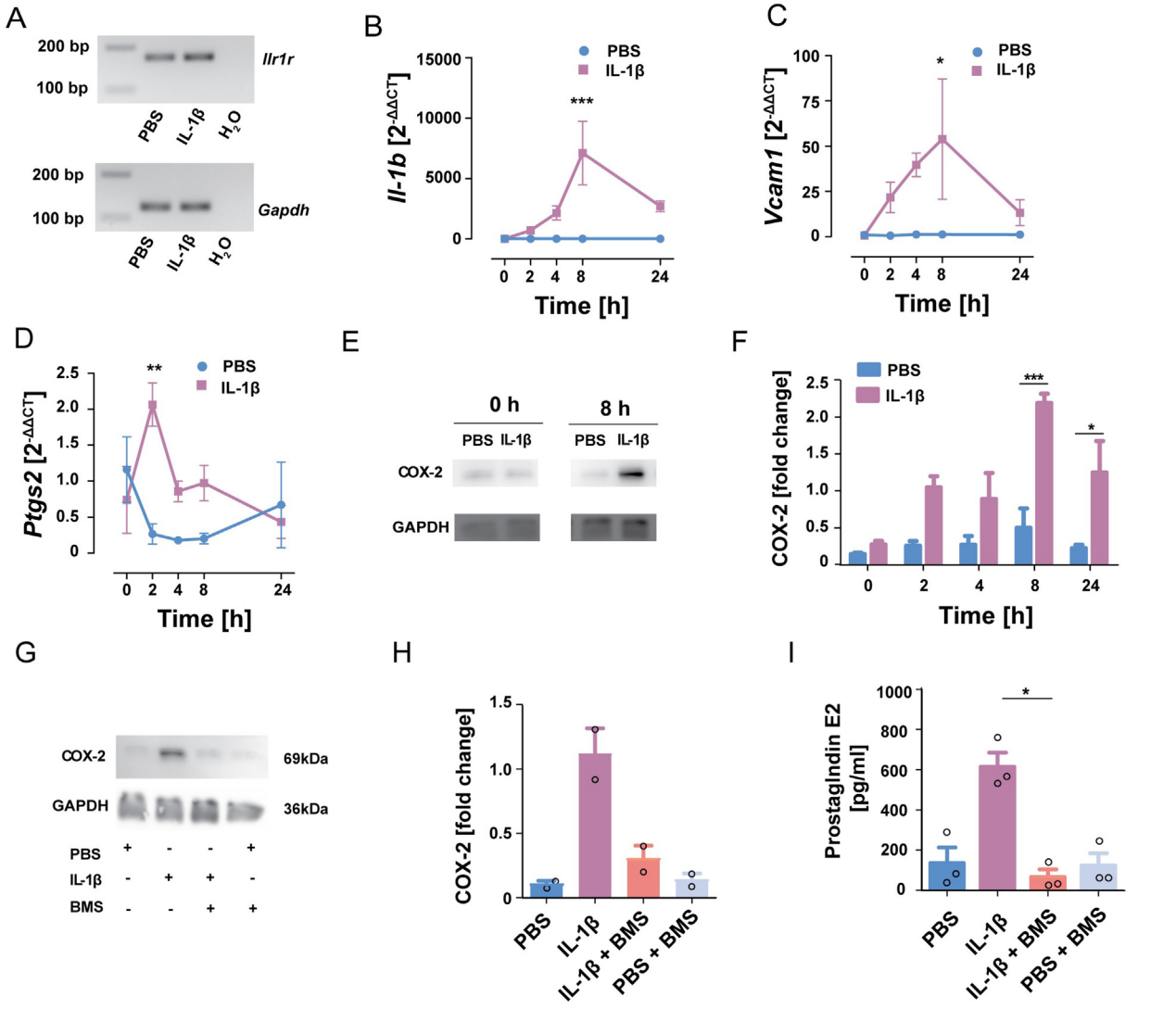

Figure 2: IL-1β stimulates the release of PGE_2 from tanycytes by activating the NF-κB pathway. (A) After treating primary tanycytes with IL-1β (0.25 μg/mL) or PBS for 24 h, *Il1r1* (172 bp) and *Gapdh* (122 bp) mRNA were detected by RT-PCR (representative images of the agarose gels). (B–D) Expression of *Il1b* (B), *Vcam1* (C), and *Ptgs2* (D) over time after IL-1β stimulation of primary tanycytes. Two-way ANOVA for treatment: *Il1b*, $F_{(1,20)} = 21.33$, $P = 0.0002$; *Vcam1*, $F_{(1,20)} = 12.09$, $P = 0.0024$; *Ptgs2*, $F_{(1,19)} = 6.11$, $P = 0.023$. $^{*}P < 0.05$, $^{**}P < 0.01$, and $^{***}P < 0.001$ (Bonferroni posttest, n = 3 independent primary cell cultures of 3 wells/experiment). (E, F) Western blots of COX-2 after IL-1β (0.25 μg/mL) stimulation of primary tanyctes. GAPDH served as a loading control. Quantification of COX-2 protein levels at various time points after IL-1β stimulation (F). Two-way ANOVA for treatment, $F_{(1,20)} = 41.57$, $P < 0.0001$. (Bonferroni posttest, n = 3 independent primary cell cultures of 3 wells/experiment). (G, H) Pretreatment with the IKK inhibitor BMS-345541 (BMS, 25 μM) blocked the induction of COX-2 by IL-1β (0.25 μg/mL) in primary tanycytes. Quantification of COX-2 protein levels (H). Two-way ANOVA; Bonferroni posttest, n = 2 independent primary cell cultures of 3 wells/experiment. (I) Quantification of PGE_2 levels in the medium showed that IL-1β stimulated PGE_2 secretion in an IKK-dependent manner. For IL-1β treatment, $F_{(1,14)} = 8.745$, $P = 0.0104$; for BMS treatment, $F_{(1,14)} = 15.48$, $P = 0.0015$; interaction, $F_{(1,14)} = 14.08$, $P = 0.0021$, posttest: $^{*}P = 0.017$ (two-way ANOVA; Bonferroni posttest, n = 3 independent primary cell cultures of 3 wells/experiment).

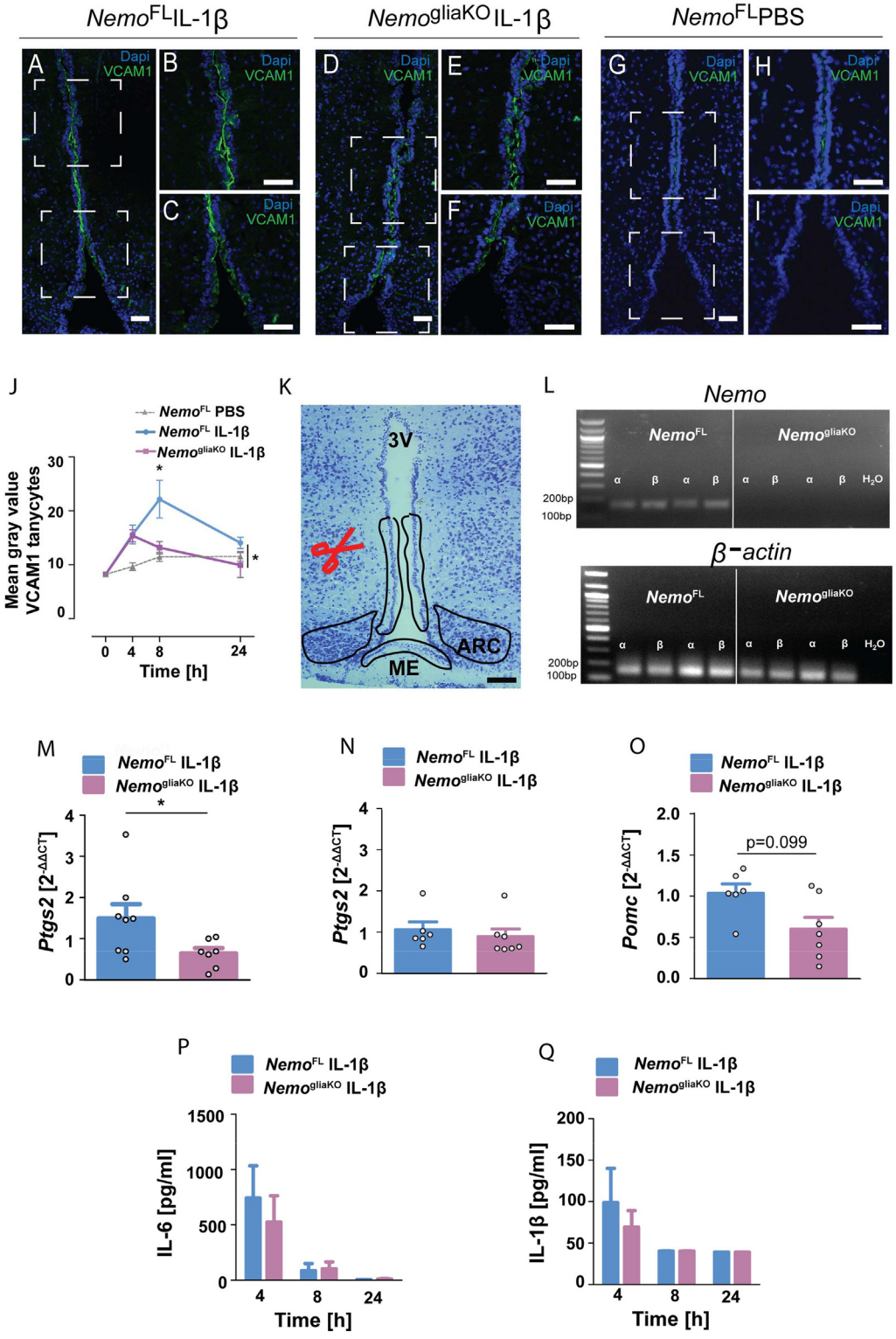

Figure 3: Glial deletion of *Nemo* (*Nemo*^{gliaKO}) interferes with the induction of NF-κB target genes by IL-1β. (A–I) Immunohistochemistry showed that IL-1β (20 μg/kg, i.v.) upregulated the NF-κB target gene VCAM1 in α-tanycytes of *Nemo*^{FL} but not of *Nemo*^{gliaKO} mice. Representative immunostainings of VCAM1 in coronal mediobasal hypothalamus (MBH) sections of *Nemo*^{FL} (A–C) and *Nemo*^{gliaKO} (D–F) mice 8 h after IL-1β treatment and PBS-treated *Nemo*^{FL} mice (G–I). (B), (C); (E), (F); and (H), (I) are higher magnifications of the boxed areas in (A), (D), and (G), respectively. Scale bar, 100 μm. (J) Quantification of VCAM1 staining in α-tanycytes projecting mainly into the VMH at various time points after IL-1β administration. Values are means ± SEM. Two-way ANOVA for genotype, $F_{(1, 29)} = 4.46$, $P = 0.044$. $^*P < 0.05$ (Bonferroni posttest, n = 7–8 animals per group). (K) Nissl-stained coronal section of the MBH showing microdissected areas of the tanycytic layer and arcuate nucleus (ARC). ME, median eminence; 3 V, 3rd ventricle; scale bar, 100 μm. (L) Representative agarose gels after RT-PCR for *Nemo* and *β-actin* in microdissected tanycytes from *Nemo*^{FL} and *Nemo*^{gliaKO} mice. (M, N) *Ptgs2* mRNA was reduced in tanycytes of *Nemo*^{gliaKO} mice in comparison to *Nemo*^{FL} controls 4 h after IL-1β treatment (M). In contrast, there was no difference in the ARC (N). $^*P < 0.05$ (Mann–Whitney test, n = 6–8 mice/group). (O) *Pomc* mRNA was reduced in tanycytes of *Nemo*^{gliaKO} mice in comparison to *Nemo*^{FL} controls 4 h after IL-1β treatment (Mann–Whitney test, n = 6–8 mice/group). (P, Q) Plasma concentrations of IL-6 (P) and IL-1β (Q) did not differ between *Nemo*^{FL} and *Nemo*^{gliaKO} animals after intravenous IL-1β injection. Values are means ± SEM (n = 6–8 mice/group).

supernatant. IL-1β stimulated PGE_2 release and BMS-345541 blocked the stimulation by IL-1β (Figure 2I). In summary, the data demonstrate that tanycytes respond to IL-1β stimulation by activating NF-κB signaling, upregulating *Ptgs2* as well as other target genes, and releasing prostanoids which can cause direct effects in the hypothalamus.

3.3. Glial *Nemo* knockout reduces NF-κB target genes in α-tanycytes

After having observed that IL-1β activates NF-κB in tanycytes, we aimed to interrupt NF-κB signaling in a cell-specific manner. IL-1β stimulates NF-κB through the canonical signaling pathway that crucially depends on NEMO [42]. To delete *Nemo*, we crossed *Nemo*^{FL} mice [25] and the *GlastCreER*^{T2} line that allows for selective gene deletion in astrocytes and tanycytes but not in microglia or neurons (Supplementary Figure 3) [26,29,43], resulting in *Nemo*^{gliaKO} mice. First, we investigated the expression of the validated NF-κB target gene VCAM1 by immunohistochemistry (Figure 3A–J). Previous studies showed that VCAM1 is upregulated in the blood–brain barrier and choroid plexus during inflammation and is involved in transmitting inflammatory signals across brain barriers [44–46]. Injecting IL-1β (20 μg/kg, i.v.) to κ-EGFP mice increased VCAM1 staining in vimentin-positive α-tanycytes in which also NF-κB was activated (Supplementary Figure 4). Upon IL-1β treatment, VCAM1 levels were lower in *Nemo*^{gliaKO} than those in *Nemo*^{FL} mice (Figure 3A–J), in accordance with the notion that the *Nemo* deletion interfered with NF-κB signaling in tanycytes. In addition, we isolated the responsive α-tanycytes, β2-tanycytes, and cells in the ARC by laser capture microdissection (LCM) (Figure 3K) to quantify mRNA expression of *Nemo* and NF-κB target genes by RT-PCR. In *Nemo*^{gliaKO} mice, *Nemo* was deleted in tanycytes, confirming the efficiency of the genetic intervention (Figure 3L). After IL-1β injection, α-tanycytes expressed lower levels of *Ptgs2* mRNA in *Nemo*^{gliaKO} mice than in *Nemo*^{FL} controls (Figure 3M), while in ARC samples, the *Ptgs2* mRNA expression did not significantly differ between the genotypes (Figure 3N). Another NF-κB target gene is the anorexigenic *Pomc* that is expressed in rat tanycytes [47]. In parallel to the *Ptgs2* mRNA expression, we observed a trend toward lower mRNA level of *Pomc* in tanycytes of *Nemo*^{gliaKO} mice after IL-1β treatment in comparison to *Nemo*^{FL} controls (Figure 3O). Hence, the glia and tanycyte-specific deletion of *Nemo* interfered with the induction of NF-κB target genes *Vcam1*, *Ptgs2*, and possibly *Pomc* that may serve tanycytes to conduct inflammatory signals into the ARC and other hypothalamic centers.

To address the possibility that *Nemo*^{FL} and *Nemo*^{gliaKO} mice could differ in the systemic inflammatory response to IL-1β, we measured cytokine plasma concentrations of IL-1β, IL-6, and TNF after IL-1β administration. TNF plasma concentrations did not rise above the detection limit of 20 pg/mL (data not shown). IL-1β and IL-6 plasma concentrations were elevated 4 h after IL-1β injection and decreased over time, independently of the genotype (Figures 3P and 3Q). These findings suggest that IL-1β administration leads to a similar inflammatory stimulus in the peripheral compartment of *Nemo*^{FL} and *Nemo*^{gliaKO} mice.

3.4. IL-1β-induced anorexia depends on glial NEMO

To determine whether the deletion of *Nemo* in glial cells leads to a metabolic phenotype under basal conditions, we evaluated the body weight under tamoxifen treatment, body weight, feeding efficiency, food and water intake, and EE and RER using indirect calorimetry, 3 weeks after the induction of the knockout (Supplementary Figures 5A–5G). These parameters did not differ between *Nemo*^{gliaKO} and *Nemo*^{FL} control mice. To investigate whether glial NEMO mediates the metabolic effects of IL-1β, we intravenously administered first PBS and after two days IL-1β (20 μg/kg) to the same animals 1 h before their active phase. In accordance with the literature, IL-1β induced anorexia in *Nemo*^{FL} mice, but this effect was blunted in *Nemo*^{gliaKO} littermates with inhibited NF-κB signaling in astrocytes and tanycytes (Figure 4A). During the first 9 h after IL-1β administration, *Nemo*^{FL} mice were severely anorexic and consumed less than 0.5 g food, whereas food ingestion was more than doubled in *Nemo*^{gliaKO} mice (Figure 4B). At later time points during the inactive phase, food intake did not differ between the groups (data not shown). Therefore, we also analyzed the other metabolic parameters in the active phase within the first 9 h after IL-1β treatment. In parallel to food intake, water consumption was diminished by IL-1β in comparison to PBS treatment (Figure 4C). *Nemo*^{gliaKO} mice only showed a trend toward more water intake than *Nemo*^{FL} littermates. Changes in food intake were reflected by the RER. As the ratio between the amount of CO_2 produced and O_2 consumed in metabolism, the RER is close to 1 when carbohydrates serve as an energy source during feeding but it drops to about 0.7 during fasting when fat metabolism meets the energy demand [48]. IL-1β reduced the RER in *Nemo*^{FL} controls in parallel to the lower food intake (Figure 4D). In contrast, glial NF-κB inhibition in *Nemo*^{gliaKO} mice led to an almost normal RER confirming that anorexia was ameliorated (Figure 4D). In addition, IL-1β treatment diminished EE in *Nemo*^{FL} mice but not in Nemo^{gliaKO} animals, although the difference between genotypes missed statistical significance (Figure 4E). Due to the lower food intake after IL-1β treatment, *Nemo*^{FL} mice showed a loss of body weight 9 h after IL-1β injection which was mitigated in *Nemo*^{gliaKO} animals (Figure 4F). As a potential explanation of the increased food intake, *Nemo*^{gliaKO} mice had higher mRNA levels of the orexigenic gene *Agrp* in LCM-dissected samples of the ARC than *Nemo*^{FL} controls after IL-1β treatment (Figure 4G), while *Pomc* and *Npy* mRNA expression did not differ in the ARC (Figure 4H,I). These data demonstrate that glial NEMO downregulates *Agrp* expression in the ARC and partially mediates the IL-1β-induced anorexia.

3.5. Fever and lethargy are not affected by glial *Nemo* knockout

To evaluate the role of glial NEMO in fever and lethargy, we determined body temperature and spontaneous home cage locomotion by telemetry. In untreated mice, body temperature and locomotion showed a circadian rhythm and did not differ between the *Nemo*^{FL} and *Nemo*^{gliaKO} genotypes (Supplementary Figure 6A and 6B). Also, when we subjected the mice to novelty stress, the transient rise in body temperature and locomotion due to the new environment was not affected by the genotype (Supplementary Figure 6C and 6D).

Injecting IL-1β or PBS led to a transient rise in body temperature in the first hour (Figure 4J). However, after 90 min, body temperature returned to baseline levels in PBS-treated *Nemo*^{FL} mice, while IL-1β significantly increased body temperature in *Nemo*^{gliaKO} and *Nemo*^{FL} mice (Figure 4J). Importantly, the second IL-1β-induced rise in body temperature was not different in *Nemo*^{gliaKO} mice compared with *Nemo*^{FL} controls. If anything, the body temperature was higher in *Nemo*^{gliaKO} than in *Nemo*^{FL} mice 60–150 min after IL-1β administration but this difference did not reach statistical significance (Figure 4J). In parallel, the cumulative activity during the first 9 h after injection decreased in response to IL-1β and again did not differ between *Nemo*^{FL} and *Nemo*^{gliaKO} mice (Figure 4K). These data show that glial NEMO is required for IL-1β-induced anorexia but not for fever and lethargy.

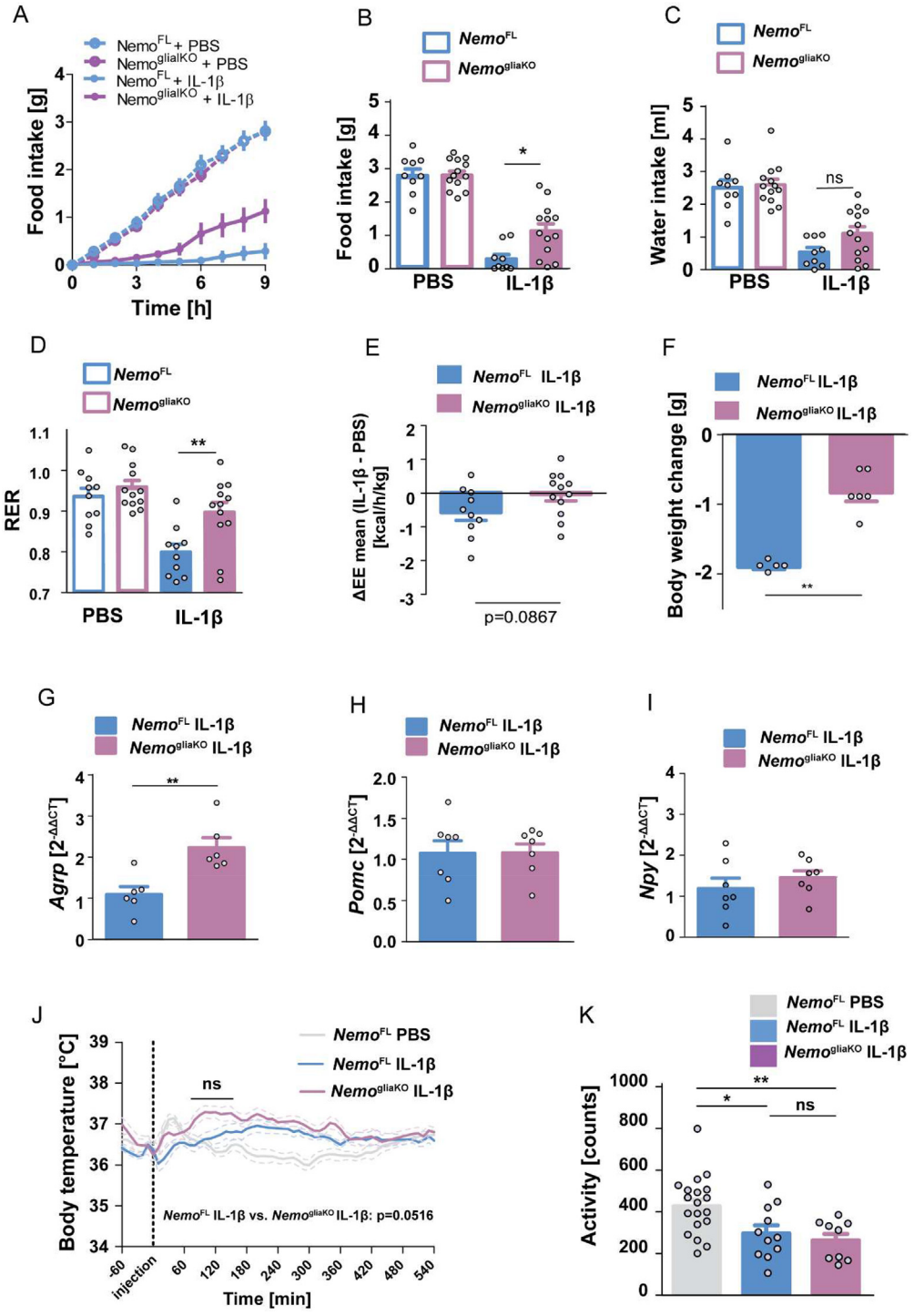

Figure 4: Glial deletion of *Nemo* (*Nemo*^{gliaKO}) mitigates IL-1β-induced anorexia but has no effect on body temperature and locomotor activity. (A) The IL-1β-induced anorexia was mitigated by the glial deletion of *Nemo*. *Nemo*^{FL} (blue) and *Nemo*^{gliaKO} mice (purple) were treated with PBS and two days later with IL-1β (20 μg/kg, i.v., 1 h before the start of the active phase). Cumulative food intake is shown. (B–D) Food ingestion (B), water intake (C), and the respiratory exchange ratio (RER, D) of *Nemo*^{FL} and *Nemo*^{gliaKO} mice over 9 h after IL-1β or PBS treatment. Means ± SEM. Repeated-measures ANOVA for the interaction between treatment and genotype; $F_{(1,20)} = 5.56$, $P = 0.029$ (B); $F_{(1,20)} = 4.82$, $P = 0.04$ (D). $^*P < 0.05$; $^{**}P < 0.01$ (Bonferroni posttest); ns, nonsignificant. (E) The reduction in energy expenditure by IL-1β (ΔEE) showed a trend toward the normalization in *Nemo*^{gliaKO} mice in comparison to *Nemo*^{FL} controls. Means ± SEM (*t*-test, n = 10–12 mice/group). (F) Loss of body weight of *Nemo*^{gliaKO} and *Nemo*^{FL} mice 9 h after IL-1β administration. $^{**}P < 0.01$ (Mann–Whitney test, n = 5–6 mice/group). (G) *Agrp* mRNA levels in the ARC were higher in *Nemo*^{gliaKO} mice than those in *Nemo*^{FL} controls 4 h after IL-1β injection. $^{**}P < 0.01$ (Mann–Whitney test, n = 6 mice/group). (H, I) Expressions of *Pomc* mRNA (H) and *Npy* mRNA (I) in ARC were unchanged in *Nemo*^{gliaKO} mice compared with *Nemo*^{FL} controls 4 h after IL-1β injection (Mann–Whitney test, n = 6 mice/group). (J) After a lag time of about 60 min, IL-1β (i.v., 20 μg/kg) increased the body temperature of *Nemo*^{FL} and *Nemo*^{gliaKO} mice in comparison to PBS-treated conditions. There was a trend toward higher body temperatures in *Nemo*^{gliaKO} than in *Nemo*^{FL} mice after IL-1β treatment. Repeated-measures ANOVA for genotype, $F_{(1,2304)} = 4.35$, $P = 0.052$. ns, nonsignificant (Bonferroni posttest). (K) In parallel, IL-1β treatment but not genotype reduced locomotor activity. One-way ANOVA, $F_{(2,38)} = 6.56$, $P = 0.0037$. $^*P < 0.05$, $^{**}P < 0.01$, ns, nonsignificant (Bonferroni posttest, n = 9–19 mice/group).

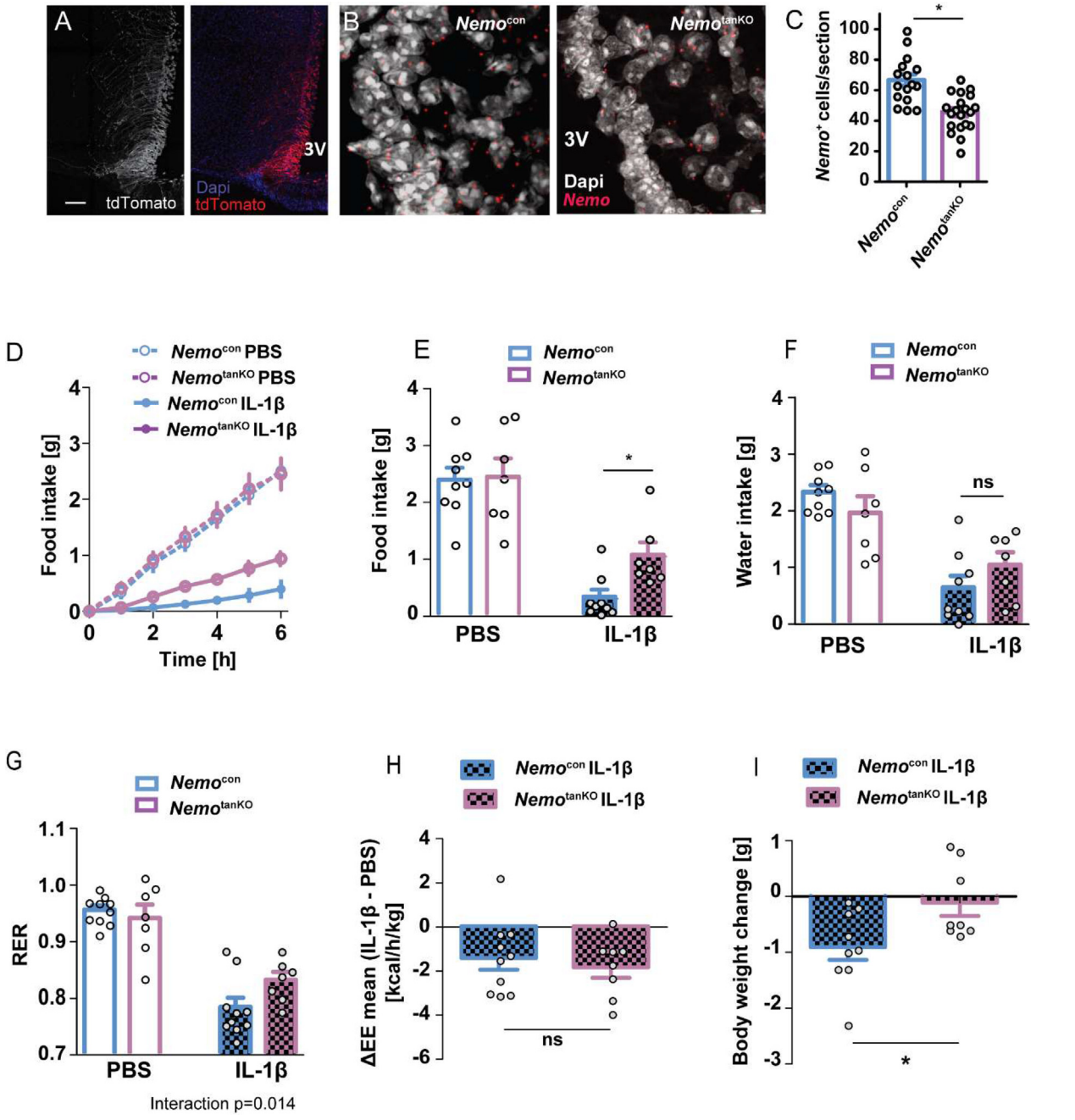

Figure 5: Tanycytic deletion of *Nemo* increases food intake after IL-1β treatment. (A).Injecting AAV-Dio2-Cre-2A-EGFP into the ventricle of Ai14 mice led to selective expression of the Cre reporter tdTomato (weight/red) in tanycytes. Blue, Dapi; scale bar, 100 μm. (B) *Nemo* mRNA (red) in the tanycyte layer. Representative *in situ* hybridization is shown. Tanycyte-specific *Nemo* knockout mice (*Nemo*^{tanKO}) were generated by injecting AAV-Dio2-Cre-2A-EGFP in the lateral ventricle of *Nemo*^{FL} mice. *Nemo*^{FL} mice that received control AAV-Dio2-EGFP are called *Nemo*^{con}. Gray, Dapi; scale bar, 1 μm. (C) Numbers of *Nemo*-positive cells in the tanycytic layer as determined by *in situ* hybridization. $^*P < 0.05$ (*t*-test). Values are means ± SEM. (D) IL-1β-induced anorexia was alleviated in *Nemo*^{tanKO} mice in comparison to *Nemo*^{FL} controls. Four weeks after virus injection, mice were treated with PBS and two days later with IL-1β (20 μg/kg). Cumulative food intake at various time points after IL-1β treatment is shown. Values are means ± SEM (n = 7–11 mice/group). (E–G) Food ingestion (E), water intake (F), and the respiratory exchange ratio (RER, G) of *Nemo*^{Con} and *Nemo*^{tanKO} mice during a period of 6 h after IL-1β or PBS treatment are depicted. Means ± SEM and individual values are shown. Repeated-measures ANOVA for interaction of treatment and genotype; $F_{(1,15)} = 4.26$, $P = 0.057$ (E); $F_{(1,15)} = 7.69$, $P = 0.014$ (G). $^*P < 0.05$ (Bonferroni posttest). (H) The reduction in energy expenditure by IL-1β (ΔEE) was similar in *Nemo*^{tanKO} mice and in *Nemo*^{con} controls. Values are means ± SEM (*t*-test, n = 8–10 mice/group). (I) Body weight loss 6 h after IL-1β administration was reduced in *Nemo*^{tanKO} mice. $^*P < 0.05$ (Mann–Whitney test, n = 8–9 mice/group).

3.6. Tanycytes mediate the IL-1β-induced anorexic effect

The experiments in the κ-EGFP reporter mice (Figure 1A–D) and the NF-κB-dependent expression of VCAM1 (Figure 3A–J) suggested that systemic IL-1β activates hypothalamic NF-κB selectively in tanycytes. To investigate whether deleting *Nemo* only in tanycytes suffices to protect animals from IL-1β-induced anorexia, we used a technique to

target tanycytes that we have recently described [29]. The approach is based on the combination of local i.c.v. administration of AAV1/2 vectors that get trapped in the ventricle wall and transduce only a few parenchymal cells and on the tanycyte-specific promoter *Dio2*. Injecting the vector AAV-Dio2-Cre-2A-EGFP into Ai14 reporter mice, in which tdTomato is a reporter of Cre activity, we confirmed the selectivity for tanycytes (Figure 5A). Four weeks after treating $Nemo^{FL}$ animals with AAV-Dio2-Cre-2A-EGFP ($Nemo^{tanKO}$) to induce recombination in tanycytes or with AAV-Dio2-EGFP as control vector ($Nemo^{Con}$), we assessed *Nemo* deletion by detecting *Nemo* mRNA on sections with *in situ* hybridization. Although the *in situ* probe partially hybridizes to the transcript derived from the recombined gene (see Methods section), we found a significant downregulation of the tanycytic *Nemo* signal in $Nemo^{tanKO}$ mice by 33% (Figure 5B,C). $Nemo^{tanKO}$ mice showed no difference in body weight, food and water intake, EE, and RER under basal conditions (Supplementary Figure 7A–7E), similar to $Nemo^{gliaKO}$ mice (Supplementary Figure 5). Also, after receiving PBS, $Nemo^{Con}$ and $Nemo^{tanKO}$ mice did not differ in food intake (Figure 5D,E). The subsequent treatment with IL-1β (20 μg/kg, i.v.) decreased the food consumption of $Nemo^{FL}$ controls as seen before. However, the IL-1β-induced anorexia was mitigated in $Nemo^{tanKO}$ mice, in which NF-κB signaling was inhibited in tanycytes (Figure 5D,E). In parallel, water intake was lower after IL-1β treatment but did not differ between the genotypes (Figure 5F). The deletion of *Nemo* in tanycytes ameliorated the RER reduction after IL-1β treatment, in accordance with the higher food intake (Figure 5G). However, IL-1β treatment reduced EE to a similar extent in $Nemo^{Con}$ and $Nemo^{tanKO}$ mice (Figure 5H). In these experiments, the body weight loss due to IL-1β was mitigated by the *Nemo* deletion in tanycytes (Figure 5I). Overall, the data indicate that NF-κB signaling in tanycytes mediates the anorexic effect of IL-1β.

4. DISCUSSION

Anorexia is an evolutionarily conserved adaptive response to inflammation and seems to promote the defense against pathogens. In chronic inflammation, this mechanism can go awry and cause life-threatening cachexia. So far, the underlying cellular mechanisms were still unclear. Our study now demonstrates a significant involvement of glial cells in the inflammation-induced anorexia mediated by the NF-κB signaling pathway. Astrocytes [49,50] and, as shown by the present study, tanycytes are responsive to IL-1β. However, after systemic administration, IL-1β activated NF-κB only in few astrocytes of the ME (Supplementary Figure 1). More prominent was the activation of NF-κB in tanycytes, microvessels, and microglia. Importantly, the tanycyte-specific deletion of *Nemo* was sufficient to interfere with IL-1β-induced anorexia. Therefore, we conclude that NF-κB signaling in tanycytes mediates inflammation-induced anorexia, at least partially. In contrast, NF-κB signaling in astrocytes has been reported to promote obesity [51–53].

Anorexia adds to the growing list of vital physiological functions that are mediated by tanycytes in the MBH [21]. On the one hand, tanycytes control neurosecretion of the hypothalamic releasing hormones GnRH and TRH [29,54]. On the other hand, they sense peripheral signals, such as leptin, glucose, and IL-1β according to this study, and transmit the message to neuroendocrine and metabolic centers in the hypothalamus [24,55]. As a common denominator, tanycytes seem to serve as a switchboard between the periphery and the hypothalamus. They are able to carry out this task due to their location at the interface between blood and CSF or brain parenchyma. From there, they send projections to essential nuclei in the MBH. As shown in this study, tanycytes projecting in the VMH and ARC respond to IL-1β and mediate the anorexigenic effect of systemic IL-1β. We suggest that the open blood–brain barrier in the circumventricular areas allows IL-1β to leave the vessel lumen, to act on tanycytes, and to stimulate NF-κB signaling. Fenestrated endothelial cells of the ME and the *pars tuberalis* or other cell types may amplify the proinflammatory signal [56] or actively transport IL-1β into the CSF [14,57]. IL-1β may also induce its own synthesis in the hypothalamus [58]. In addition to IL-1β, systemically administered LPS activates NF-κB in tanycytes [59] and induces anorexia. As the anorexic effect of peripheral LPS does not depend on IL1R1 [60], LPS likely acts directly on tanycytes to induce a similar cascade of events as IL-1β.

The role of tanycytes in transmitting inflammatory signals from the periphery to the hypothalamus seems to be specifically focused on anorexia, because tanycytic NF-κB did not modulate fever and lethargy. In contrast, endothelial NF-κB mediates IL-1β-induced fever and lethargy but not food intake [17]. Thus, independent mechanisms underlie the various facets of the sickness response [17,60,61]. These findings also illustrate that anorexia does not simply reflect an unspecific secondary effect of general sickness but rather an independent effect of systemic inflammation.

NF-κB signaling in tanycytes emerges as an attractive target to ameliorate cachexia and to reduce mortality in cancer and chronic infections. Since inhibiting NF-κB is an effective treatment strategy to stop tumor progression [62], blockers of NF-κB signaling may provide dual benefit for patients with malignant diseases. Alternative targets for treating cachexia are IL-1 itself or COX-2 as a downstream gene of NF-κB in tanycytes. Clinical trials and experimental studies show that an anti-IL-1 antibody and COX-2 inhibitors improve anorexia in infections, cancer cachexia, and systemic inflammation [12,13,63–65]. The early phase of anorexia is mediated by COX-1, while COX-2 seems to maintain anorexia [13]. Interestingly, this time course is also reflected in our results. After IL-1β treatment, both $Nemo^{gliaKO}$ and $Nemo^{tanKO}$ mice started to eat again earlier than control animals, indicating a predominant effect of the tanycytic COX-2 expression in the later phase of anorexia. Supporting the relevance of tanycytes, cell-specific knockouts of COX-2 in endothelia, neurons, and myeloid cells failed to inhibit LPS-induced anorexia [19]. The localization of tanycytes in the ventricle wall may explain why prostaglandin levels are elevated in the CSF during inflammation [60,66]. When injected into the ventricle, PGE_2 or PGF2α has an anorexic effect [67,68]. However, the specific prostaglandin downstream of COX-2 that mediates anorexia differs between species and even mouse strains [65,69–71]. Parallel to the NF-κB–COX-2–prostaglandin pathway, there are several other potential mechanisms of how tanycytes could mediate anorexia. A candidate is the anorexic gliotransmitter ACBP that is expressed in tanycytes, despite the observation that deletion of ACBP in tanycytes does not affect food intake and body weight on a high-fat diet [72]. In accordance with previous work, we detected *Pomc* mRNA in tanycytes [47]. *Pomc* showed a trend toward lower expression in tanycytes of $Nemo^{gliaKO}$ mice after systemic IL-1β treatment. Regulation of *Pomc* expression by NF-κB in neurons of the ARC seems to be functionally relevant because the deletion of the β subunit of IKK in POMC-positive cells reduced inflammation-induced anorexia [73]. After translation, POMC is cleaved to the active and anorectic peptide α-MSH, which was detected in low concentrations in tanycytes of rats [47]. An IL-1β-dependent release of α-MSH by tanycytes could mediate the direct anorexic effect of inflammation.

Tanycytes are able to modulate the expression of orexigenic and anorexigenic peptides in the hypothalamus and thereby food intake [74]. IL-1β-treated $Nemo^{gliaKO}$ mice had a higher expression of *Agrp*

mRNA in the ARC compared with *Nemo*^{FL} mice. AGRP likely enhances food intake after IL-1β administration, since the parallel injection of AGRP into the CSF abolished anorexia induced by IL-1β [75]. If the release of α-MSH by tanycytes contributes to the IL-1β-induced anorexia, upregulation of AGRP could inhibit the α-MSH effects, since AGRP is a direct antagonist of α-MSH [76]. AGRP neurons also project into the bed nucleus of stria terminalis (BNST), which is an important nucleus for feeding behavior [77]. Upon stimulation, AGRP neurons release GABA and, by inhibiting PKC-δ neurons in the oval part of the BNST, increase food intake under IL-1β and LPS treatment [77,78]. The physiological importance of the central response to inflammation suggests that, in addition to the tanycytic pathway, other mechanisms may contribute to anorexia. Such a scenario would explain why the IL-1β-mediated anorexia was only partly rescued by tanycytic NEMO deficiency (Figure 4 and Figure 5). The vagus nerve expresses IL-1R1 and can deliver proinflammatory signals from the periphery to the brainstem [79–81]. Vagal afferents end in the nucleus of the solitary tract that is connected to the parabrachial nucleus containing an "emergency circuit" that mediates cancer-induced anorexia [82,83].

5. CONCLUSIONS

This study has identified a tanycytic cell population, which directly senses peripheral IL-1β. Triggered by systemic inflammation, tanycytes mount an NF-κB response, express COX-2, release prostaglandins, and modulate orexigenic and anorexigenic peptides in the hypothalamus. Inhibition of the NF-κB pathway in tanycytes mitigated anorexia *in vivo*. Overall, tanycytes emerge as an important mediator of inflammation-induced anorexia.

AUTHORS' CONTRIBUTIONS

M.S. conceived the study; M.B., H.M.F., D.E., V.P., and M.S. designed the experiments; M.B., H.M.F., K.S., A.B., and D.E. performed and analyzed telemetric measurements; M.B., S.G., and V.P. cultured primary tanycytes and performed cell culture experiments; M.B. and H.M.F. investigated mice by indirect calorimetry; M.B., H.M.F., K.S., A.B., and D.E. performed feeding studies; M.B., H.M.F., S.S., A.Z., V.N., J.W., and A.B. performed immunohistochemistry; R.H., R.S.U., N.Q., and X.L. provided essential tools and know-how on IL1R1 and NF-κB signaling; M.B., H.M.F., S.S., and M.S. drafted the manuscript. All authors corrected the manuscript.

ACKNOWLEDGMENTS

We would like to thank Ines Stölting and Frauke Spiecker for expert technical help, Kathrin Kalies for kind support with laser microdissection, Manolis Pasparakis, Cologne, for providing *Nemo*^{FL} mice, Magdalena Götz, Munich, for providing *Glast-CreER*^{T2} animals, and Martin Wessendorf, Minneapolis, for providing ppTRH antibody. This project has received funding from the Deutsche Forschungsgemeinschaft (GRK1957, T-CRC 134 to M.S.; SPP1629, MU 3743/1-1 to H.M.F.); the Swedish Research Council (#07879 and #20725), the Swedish Brain Foundation, the Swedish Cancer Foundation (#2016/585) to A.B.; the Agence Nationale de la Recherche (ANR-15-CE14-0025-01, ANR-16-CE37-0006-02) to V.P.; and the European Research Council (ERC) under the European Union's Horizon 2020 research and innovation programme (grant agreement No. 810331) to V.*P. and* M.S. R.H. received funding from the Velux Stiftung, Switzerland.

CONFLICT OF INTEREST

None declared.

APPENDIX A. SUPPLEMENTARY DATA

Supplementary data to this article can be found online at https://doi.org/10.1016/j.molmet.2020.101022.

REFERENCES

[1] Plata-Salaman, C.R., 1996. Anorexia during acute and chronic disease. Nutrition 12(2):69–78.
[2] Baracos, V.E., Martin, L., Korc, M., Guttridge, D.C., Fearon, K.C.H., 2018. Cancer-associated cachexia. Natural Resources Diseases Primers 4:17105.
[3] Gautron, L., Laye, S., 2009. Neurobiology of inflammation-associated anorexia. Frontiers in Neuroscience 3:59.
[4] Morley, J.E., Thomas, D.R., Wilson, M.M., 2006. Cachexia: pathophysiology and clinical relevance. American Journal of Clinical Nutrition 83(4):735–743.
[5] Hotamisligil, G.S., Erbay, E., 2008. Nutrient sensing and inflammation in metabolic diseases. Nature Reviews Immunology 8(12):923–934.
[6] Wang, A., Huen, Sarah C., Luan, Harding H., Yu, S., Zhang, C., Gallezot, J.-D., et al., 2016. Opposing effects of fasting metabolism on tissue tolerance in bacterial and viral inflammation. Cell 166(6):1512–1525 e1512.
[7] Rao, S., Schieber, A.M., O'Connor, C.P., Leblanc, M., Michel, D., Ayres, J.S., 2017. Pathogen-mediated inhibition of anorexia promotes host survival and transmission. Cell 168(3):503–516 e512.
[8] Konsman, J.P., Parnet, P., Dantzer, R., 2002. Cytokine-induced sickness behaviour: mechanisms and implications. Trends in Neurosciences 25(3):154–159.
[9] Liu, X., Nemeth, D.P., McKim, D.B., Zhu, L., DiSabato, D.J., Berdysz, O., et al., 2019. Cell-type-specific interleukin 1 receptor 1 signaling in the brain regulates distinct neuroimmune activities. Immunity.
[10] Ruud, J., Backhed, F., Engblom, D., Blomqvist, A., 2010. Deletion of the gene encoding MyD88 protects from anorexia in a mouse tumor model. Brain, Behavior, and Immunity 24(4):554–557.
[11] Ogimoto, K., Harris Jr., M.K., Wisse, B.E., 2006. MyD88 is a key mediator of anorexia, but not weight loss, induced by lipopolysaccharide and interleukin-1 beta. Endocrinology 147(9):4445–4453.
[12] Langhans, W., 2007. Signals generating anorexia during acute illness. Proceedings of the Nutrition Society 66(3):321–330.
[13] Swiergiel, A.H., Dunn, A.J., 2002. Distinct roles for cyclooxygenases 1 and 2 in interleukin-1-induced behavioral changes. Journal of Pharmacology and Experimental Therapeutics 302(3):1031–1036.
[14] Banks, W.A., Ortiz, L., Plotkin, S.R., Kastin, A.J., 1991. Human interleukin (IL) 1 alpha, murine IL-1 alpha and murine IL-1 beta are transported from blood to brain in the mouse by a shared saturable mechanism. Journal of Pharmacology and Experimental Therapeutics 259(3):988–996.
[15] Engström, L., Ruud, J., Eskilsson, A., Larsson, A., Mackerlova, L., Kugelberg, U., et al., 2012. Lipopolysaccharide-induced fever depends on prostaglandin E2 production specifically in brain endothelial cells. Endocrinology.
[16] Wilhelms, D.B., Kirilov, M., Mirrasekhian, E., Eskilsson, A., Kugelberg, U.Ö., Klar, C., et al., 2014. Deletion of prostaglandin E2 synthesizing enzymes in brain endothelial cells attenuates inflammatory fever. Journal of Neuroscience 34(35):11684–11690.
[17] Ridder, D.A., Lang, M.F., Salinin, S., Roderer, J.P., Struss, M., Maser-Gluth, C., et al., 2011. TAK1 in brain endothelial cells mediates fever and lethargy. Journal of Experimental Medicine 208(13):2615–2623.
[18] Blomqvist, A., Engblom, D., 2018. Neural mechanisms of inflammation-induced fever. The Neuroscientist 24(4):381–399.
[19] Nilsson, A., Wilhelms, D.B., Mirrasekhian, E., Jaarola, M., Blomqvist, A., Engblom, D., 2017. Inflammation-induced anorexia and fever are elicited by distinct prostaglandin dependent mechanisms, whereas conditioned taste

aversion is prostaglandin independent. Brain, Behavior, and Immunity 61: 236–243.

[20] Fritz, M., Klawonn, A.M., Nilsson, A., Singh, A.K., Zajdel, J., Wilhelms, D.B., et al., 2016. Prostaglandin-dependent modulation of dopaminergic neurotransmission elicits inflammation-induced aversion in mice. Journal of Clinical Investigation 126(2):695–705.

[21] Prevot, V., Dehouck, B., Sharif, A., Ciofi, P., Giacobini, P., Clasadonte, J., 2018. The versatile tanycyte: a hypothalamic integrator of reproduction and energy metabolism. Endocrine Reviews 39(3):333–368.

[22] Barahona, M.J., Llanos, P., Recabal, A., Escobar-Acuna, K., Elizondo-Vega, R., Salgado, M., et al., 2018. Glial hypothalamic inhibition of GLUT2 expression alters satiety, impacting eating behavior. Glia 66(3):592–605.

[23] Collden, G., Balland, E., Parkash, J., Caron, E., Langlet, F., Prevot, V., et al., 2015. Neonatal overnutrition causes early alterations in the central response to peripheral ghrelin. Molecular Metabolism 4(1):15–24.

[24] Balland, E., Dam, J., Langlet, F., Caron, E., Steculorum, S., Messina, A., et al., 2014. Hypothalamic tanycytes are an ERK-gated conduit for leptin into the brain. Cell Metabolism 19(2):293–301.

[25] Schmidt-Supprian, M., Bloch, W., Courtois, G., Addicks, K., Israel, A., Rajewsky, K., et al., 2000. NEMO/IKK gamma-deficient mice model incontinentia pigmenti. Molecular Cell 5(6):981–992.

[26] Mori, T., Tanaka, K., Buffo, A., Wurst, W., Kühn, R., Götz, M., 2006. Inducible gene deletion in astroglia and radial glia—a valuable tool for functional and lineage analysis. Glia 54(1):21–34.

[27] Tomann, P., Paus, R., Millar, S.E., Scheidereit, C., Schmidt-Ullrich, R., 2016. Lhx2 is a direct NF-kappaB target gene that promotes primary hair follicle placode down-growth. Development 143(9):1512–1522.

[28] Liu, X., Yamashita, T., Chen, Q., Belevych, N., McKim, D.B., Tarr, A.J., et al., 2015. Interleukin 1 type 1 receptor restore: a genetic mouse model for studying interleukin 1 receptor-mediated effects in specific cell types. Journal of Neuroscience 35(7):2860–2870.

[29] Müller-Fielitz, H., Stahr, M., Bernau, M., Richter, M., Abele, S., Krajka, V., et al., 2017. Tanycytes control the hormonal output of the hypothalamic-pituitary-thyroid axis. Nature Communications 8(1):484.

[30] Madisen, L., Zwingman, T.A., Sunkin, S.M., Oh, S.W., Zariwala, H.A., Gu, H., et al., 2010. A robust and high-throughput Cre reporting and characterization system for the whole mouse brain. Nature Neuroscience 13(1):133–140.

[31] Prevot, V., Cornea, A., Mungenast, A., Smiley, G., Ojeda, S.R., 2003. Activation of erbB-1 signaling in tanycytes of the median eminence stimulates transforming growth factor beta1 release via prostaglandin E2 production and induces cell plasticity. Journal of Neuroscience 23(33):10622–10632.

[32] Langlet, F., Levin, B.E., Luquet, S., Mazzone, M., Messina, A., Dunn-Meynell, A.A., et al., 2013. Tanycytic VEGF-A boosts blood-hypothalamus barrier plasticity and access of metabolic signals to the arcuate nucleus in response to fasting. Cell Metabolism 17(4):607–617.

[33] Giaretta, P.R., Rech, R.R., Guard, B.C., Blake, A.B., Blick, A.K., Steiner, J.M., et al., 2018. Comparison of intestinal expression of the apical sodium-dependent bile acid transporter between dogs with and without chronic inflammatory enteropathy. Journal of Veterinary Internal Medicine 32(6):1918–1926.

[34] Ericsson, A., Liu, C., Hart, R.P., Sawchenko, P.E., 1995. Type 1 interleukin-1 receptor in the rat brain: distribution, regulation, and relationship to sites of IL-1-induced cellular activation. Journal of Comparative Neurology 361(4):681–698.

[35] Dinarello, C.A., 1996. Biologic basis for interleukin-1 in disease. Blood 87(6): 2095–2147.

[36] Engström, L., Ruud, J., Eskilsson, A., Larsson, A., Mackerlova, L., Kugelberg, U., et al., 2012. Lipopolysaccharide-induced fever depends on prostaglandin E2 production specifically in brain endothelial cells. Endocrinology 153(10):4849–4861.

[37] Jung, H.Y., Yoo, D.Y., Nam, S.M., Kim, J.W., Kim, W., Kwon, H.J., et al., 2019. Postnatal changes in constitutive cyclooxygenase2 expression in the mice hippocampus and its function in synaptic plasticity. Molecular Medicine Reports 19(3):1996–2004.

[38] Burke, J.R., Pattoli, M.A., Gregor, K.R., Brassil, P.J., MacMaster, J.F., McIntyre, K.W., et al., 2003. BMS-345541 is a highly selective inhibitor of I kappa B kinase that binds at an allosteric site of the enzyme and blocks NF-kappa B-dependent transcription in mice. Journal of Biological Chemistry 278(3):1450–1456.

[39] Eskilsson, A., Tachikawa, M., Hosoya, K., Blomqvist, A., 2014. Distribution of microsomal prostaglandin E synthase-1 in the mouse brain. Journal of Comparative Neurology 522(14):3229–3244.

[40] De Seranno, S., Estrella, C., Loyens, A., Cornea, A., Ojeda, S.R., Beauvillain, J.C., et al., 2004. Vascular endothelial cells promote acute plasticity in ependymoglial cells of the neuroendocrine brain. Journal of Neuroscience 24(46):10353–10363.

[41] de Seranno, S., d'Anglemont de Tassigny, X., Estrella, C., Loyens, A., Kasparov, S., Leroy, D., et al., 2010. Role of estradiol in the dynamic control of tanycyte plasticity mediated by vascular endothelial cells in the median eminence. Endocrinology 151(4):1760–1772.

[42] Yamaoka, S., Courtois, G., Bessia, C., Whiteside, S.T., Weil, R., Agou, F., et al., 1998. Complementation cloning of NEMO, a component of the IkappaB kinase complex essential for NF-kappaB activation. Cell 93(7):1231–1240.

[43] Robins, S.C., Stewart, I., McNay, D.E., Taylor, V., Giachino, C., Goetz, M., et al., 2013. alpha-Tanycytes of the adult hypothalamic third ventricle include distinct populations of FGF-responsive neural progenitors. Nature Communications 4:2049.

[44] Engelhardt, B., Conley, F.K., Butcher, E.C., 1994. Cell adhesion molecules on vessels during inflammation in the mouse central nervous system. Journal of Neuroimmunology 51(2):199–208.

[45] Steffen, B.J., Breier, G., Butcher, E.C., Schulz, M., Engelhardt, B., 1996. ICAM-1, VCAM-1, and MAdCAM-1 are expressed on choroid plexus epithelium but not endothelium and mediate binding of lymphocytes in vitro. American Journal Of Pathology 148(6):1819–1838.

[46] Yousef, H., Czupalla, C.J., Lee, D., Chen, M.B., Burke, A.N., Zera, K.A., et al., 2019. Aged blood impairs hippocampal neural precursor activity and activates microglia via brain endothelial cell VCAM1. Nature Medicine 25(6):988–1000.

[47] Wittmann, G., Farkas, E., Szilvasy-Szabo, A., Gereben, B., Fekete, C., Lechan, R.M., 2017. Variable proopiomelanocortin expression in tanycytes of the adult rat hypothalamus and pituitary stalk. Journal of Comparative Neurology 525(3):411–441.

[48] Tschöp, M.H., Speakman, J.R., Arch, J.R., Auwerx, J., Brüning, J.C., Chan, L., et al., 2012. A guide to analysis of mouse energy metabolism. Nature Methods 9(1):57–63.

[49] Ito, H., Yamamoto, N., Arima, H., Hirate, H., Morishima, T., Umenishi, F., et al., 2006. Interleukin-1beta induces the expression of aquaporin-4 through a nuclear factor-kappaB pathway in rat astrocytes. Journal of Neurochemistry 99(1):107–118.

[50] Molina-Holgado, E., Ortiz, S., Molina-Holgado, F., Guaza, C., 2000. Induction of COX-2 and PGE(2) biosynthesis by IL-1beta is mediated by PKC and mitogen-activated protein kinases in murine astrocytes. British Journal of Pharmacology 131(1):152–159.

[51] Garcia-Caceres, C., Balland, E., Prevot, V., Luquet, S., Woods, S.C., Koch, M., et al., 2019. Role of astrocytes, microglia, and tanycytes in brain control of systemic metabolism. Nature Neuroscience 22(1):7–14.

[52] Douglass, J.D., Dorfman, M.D., Fasnacht, R., Shaffer, L.D., Thaler, J.P., 2017. Astrocyte IKKbeta/NF-kappaB signaling is required for diet-induced obesity and hypothalamic inflammation. Molecular Metabolism 6(4):366–373.

[53] Zhang, Y., Reichel, J.M., Han, C., Zuniga-Hertz, J.P., Cai, D., 2017. Astrocytic process plasticity and IKKbeta/NF-kappaB in central control of blood glucose, blood pressure, and body weight. Cell Metabolism 25(5):1091–1102 e1094.

[54] Parkash, J., Messina, A., Langlet, F., Cimino, I., Loyens, A., Mazur, D., et al., 2015. Semaphorin7A regulates neuroglial plasticity in the adult hypothalamic median eminence. Nature Communications 6:6385.

[55] Benford, H., Bolborea, M., Pollatzek, E., Lossow, K., Hermans-Borgmeyer, I., Liu, B., et al., 2017. A sweet taste receptor-dependent mechanism of glucosensing in hypothalamic tanycytes. Glia 65(5):773—789.

[56] Knoll, J.G., Krasnow, S.M., Marks, D.L., 2017. Interleukin-1beta signaling in fenestrated capillaries is sufficient to trigger sickness responses in mice. Journal of Neuroinflammation 14(1):219.

[57] Erickson, M.A., Banks, W.A., 2018. Neuroimmune axes of the blood-brain barriers and blood-brain interfaces: bases for physiological regulation, disease states, and pharmacological interventions. Pharmacological Reviews 70(2):278—314.

[58] Skelly, D.T., Hennessy, E., Dansereau, M.A., Cunningham, C., 2013. A systematic analysis of the peripheral and CNS effects of systemic LPS, IL-1beta, [corrected] TNF-alpha and IL-6 challenges in C57BL/6 mice. PloS One 8(7):e69123.

[59] de Vries, E.M., Nagel, S., Haenold, R., Sundaram, S.M., Pfrieger, F.W., Fliers, E., et al., 2016. The role of hypothalamic NF-kappaB signaling in the response of the HPT-Axis to acute inflammation in female mice. Endocrinology 157(7):2947—2956.

[60] Matsuwaki, T., Shionoya, K., Ihnatko, R., Eskilsson, A., Kakuta, S., Dufour, S., et al., 2017. Involvement of interleukin-1 type 1 receptors in lipopolysaccharide-induced sickness responses. Brain, Behavior, and Immunity 66(Supplement C):165—176.

[61] Serrats, J., Schiltz, J.C., García-Bueno, B., van Rooijen, N., Reyes, T.M., Sawchenko, P.E., 2010. Dual roles for perivascular macrophages in immune-to-brain signaling. Neuron 65(1):94—106.

[62] Taniguchi, K., Karin, M., 2018. NF-kappaB, inflammation, immunity and cancer: coming of age. Nature Reviews Immunology 18(5):309—324.

[63] Prado, B.L., Qian, Y., 2019. Anti-cytokines in the treatment of cancer cachexia. Annals of Palliative Medicine 8(1):67—79.

[64] Maccio, A., Madeddu, C., Gramignano, G., Mulas, C., Floris, C., Sanna, E., et al., 2012. A randomized phase III clinical trial of a combined treatment for cachexia in patients with gynecological cancers: evaluating the impact on metabolic and inflammatory profiles and quality of life. Gynecologic Oncology 124(3):417—425.

[65] Nilsson, A., Elander, L., Hallbeck, M., Örtegren Kugelberg, U., Engblom, D., Blomqvist, A., 2017. The involvement of prostaglandin E2 in interleukin-1β evoked anorexia is strain dependent. Brain, Behavior, and Immunity 60: 27—31.

[66] Eskilsson, A., Matsuwaki, T., Shionoya, K., Mirrasekhian, E., Zajdel, J., Schwaninger, M., et al., 2017. Immune-induced fever is dependent on local but not generalized prostaglandin E2 synthesis in the brain. Journal of Neuroscience 37(19):5035—5044.

[67] Skibicka, K.P., Alhadeff, A.L., Leichner, T.M., Grill, H.J., 2011. Neural controls of prostaglandin 2 pyrogenic, tachycardic, and anorexic actions are anatomically distributed. Endocrinology 152(6):2400—2408.

[68] Tachibana, T., Nakai, Y., Makino, R., Khan, M.S.I., Cline, M.A., 2017. Effect of central and peripheral injection of prostaglandin E2 and F2α on feeding and the crop-emptying rate in chicks. Prostaglandins & Other Lipid Mediators 130:30—37.

[69] Ohinata, K., Suetsugu, K., Fujiwara, Y., Yoshikawa, M., 2006. Activation of prostaglandin E receptor EP4 subtype suppresses food intake in mice. Prostaglandins & Other Lipid Mediators 81(1—2):31—36.

[70] Pecchi, E., Dallaporta, M., Thirion, S., Salvat, C., Berenbaum, F., Jean, A., et al., 2006. Involvement of central microsomal prostaglandin E synthase-1 in IL-1beta-induced anorexia. Physiological Genomics 25(3):485—492.

[71] Smith, W.L., Urade, Y., Jakobsson, P.J., 2011. Enzymes of the cyclooxygenase pathways of prostanoid biosynthesis. Chemical Reviews 111(10):5821—5865.

[72] Bouyakdan, K., Martin, H., Lienard, F., Budry, L., Taib, B., Rodaros, D., et al., 2019. The gliotransmitter ACBP controls feeding and energy homeostasis via the melanocortin system. Journal of Clinical Investigation 129(6):2417—2430.

[73] Jang, P.G., Namkoong, C., Kang, G.M., Hur, M.W., Kim, S.W., Kim, G.H., et al., 2010. NF-kappaB activation in hypothalamic pro-opiomelanocortin neurons is essential in illness- and leptin-induced anorexia. Journal of Biological Chemistry 285(13):9706—9715.

[74] Uranga, R.M., Millan, C., Barahona, M.J., Recabal, A., Salgado, M., Martinez, F., et al., 2017. Adenovirus-mediated suppression of hypothalamic glucokinase affects feeding behavior. Scientific Reports 7(1):3697.

[75] DeBoer, M.D., Scarlett, J.M., Levasseur, P.R., Grant, W.F., Marks, D.L., 2009. Administration of IL-1beta to the 4th ventricle causes anorexia that is blocked by agouti-related peptide and that coincides with activation of tyrosine-hydroxylase neurons in the nucleus of the solitary tract. Peptides 30(2): 210—218.

[76] Ollmann, M.M., Wilson, B.D., Yang, Y.K., Kerns, J.A., Chen, Y., Gantz, I., et al., 1997. Antagonism of central melanocortin receptors in vitro and in vivo by agouti-related protein. Science 278(5335):135—138.

[77] Betley, J.N., Cao, Z.F., Ritola, K.D., Sternson, S.M., 2013. Parallel, redundant circuit organization for homeostatic control of feeding behavior. Cell 155(6): 1337—1350.

[78] Wang, Y., Kim, J., Schmit, M.B., Cho, T.S., Fang, C., Cai, H., 2019. A bed nucleus of stria terminalis microcircuit regulating inflammation-associated modulation of feeding. Nature Communications 10(1):2769.

[79] Bret-Dibat, J.L., Bluthe, R.M., Kent, S., Kelley, K.W., Dantzer, R., 1995. Lipopolysaccharide and interleukin-1 depress food-motivated behavior in mice by a vagal-mediated mechanism. Brain, Behavior, and Immunity 9(3): 242—246.

[80] Ek, M., Engblom, D., Saha, S., Blomqvist, A., Jakobsson, P.J., Ericsson-Dahlstrand, A., 2001. Inflammatory response: pathway across the blood-brain barrier. Nature 410(6827):430—431.

[81] Hosoi, T., Okuma, Y., Matsuda, T., Nomura, Y., 2005. Novel pathway for LPS-induced afferent vagus nerve activation: possible role of nodose ganglion. Autonomic Neuroscience 120(1—2):104—107.

[82] Campos, C.A., Bowen, A.J., Han, S., Wisse, B.E., Palmiter, R.D., Schwartz, M.W., 2017. Cancer-induced anorexia and malaise are mediated by CGRP neurons in the parabrachial nucleus. Nature Neuroscience 20(7):934—942.

[83] Ruud, J., Blomqvist, A., 2007. Identification of rat brainstem neuronal structures activated during cancer-induced anorexia. Journal of Comparative Neurology 504(3):275—286.

